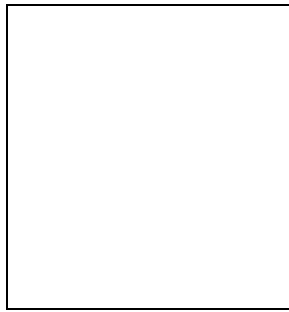


THE ANALYSIS OF GIANT H II REGIONS USING PHOTOIONIZATION MODELS

G. Stasińska DAEC, Observatoire de Meudon, France ¹



Abstract

After briefly reviewing the impact of various parameters on photoionization models, we illustrate the importance of the nebular geometry by two examples: we first compare the results from models with thin shell and full sphere geometry, and we study the influence of a diffuse ionized medium in the integrated spectra of galaxies at large redshift. Finally, we show how the calibration of the strong line method for deriving oxygen abundances depends on the assumed average properties of the ionizing star cluster and on the density distribution of the nebular gas.

1 Introduction

In the past, the analysis of giant H II regions relied on single star photoionization models. Recent advances in stellar evolution and population synthesis made it possible to build models of H II regions that are ionized by star clusters ([22], [23], [5], [10], [11], [13], [35]). Such models are helpful in the quest of the best diagnostics of giant H II regions and of the populations of hot stars embedded in them [36].

After a short introduction to photoionization modelling, we will mainly address two points. One concerns the influence of the nebular density structure. The other concerns the strong line method for deriving elemental abundances. This method has already been widely discussed in the literature, but deserves further attention because it is the only possible way to derive abundances in low surface brightness systems as well as in distant galaxies.

¹ to appear in “Dwarf Galaxies and Cosmology”, eds. Cayatte et al., Editions Frontieres

2 Photoionization modelling in brief

The primary parameters defining a model are (i) the oxygen abundance (oxygen usually provides most of the cooling and can be considered as the element defining the metallicity Z), (ii) the mean effective temperature $\langle T_{eff} \rangle$ of the ionizing radiation field (to first order, it can be characterized by the ratio Q_{He^o} / Q_{H^o} of the total number of photons above 24.6 and 13.6 eV, and (iii) the ionization parameter U_S whose definition for a spherical nebula of constant density is $U_S = Q_{H^o} / (4\pi R_S^2 nc)$ where R_S is the Strömgren radius, n is the gas density and c the speed of light.

The intensities of the emission lines are proportional to the ionic populations of the elements producing them, but are strongly modulated by the electron temperature. The electron temperature results from a balance between the energy gains (due to ionization of hydrogen and helium, and essentially fixed by the effective temperature) and the energy losses (mainly due to line emission from the "metals", i.e. the elements heavier than H and He, except for the lowest metallicities where hydrogen losses become dominant). The ionization parameter sets the distribution of the various ions within the nebula, once the radiation field is specified.

Among the secondary parameters are: (i) the relative abundances of the elements in the gas with respect to oxygen, (ii) the possible presence of dust and its composition, (iii) the details of the energy distribution of the stellar ionizing photons, and (iv) the gas density distribution and the location of the ionizing stars with respect to the gas.

The species whose abundance variations affect the thermal balance most are nitrogen, carbon, and the refractory elements. The N/O and C/O ratios are expected to vary from one object to another since nitrogen and carbon are not produced in the same nucleosynthetic sites as oxygen. If abundant, nitrogen and carbon contribute significantly to the cooling of the gas. Refractory elements like Si, Mg, Fe may be depleted in the gas phase if dust is present, and deprive it from a cooling source which becomes important at high metallicities [14].

The direct effects of dust (apart from reddening) are mainly to compete with gas for the absorption of photons [26] but, as shown by [1], dust also participates in the heating or the cooling of the gas. These effects strongly depend on the physical conditions inside the nebula and are difficult to model in detail, but they are of secondary importance in the thermal balance.

The energy distribution of the ionizing radiation field is dictated by the population of ionizing stars and the properties of their atmospheres. Even for a *given* mean effective temperature (or a mean Q_{He^o} / Q_{H^o}), the stellar energy distribution influences the emission line properties by affecting the ionization structure of the various elements [38]. A review of the impact of stellar evolution and atmospheres can be found in [12].

The effect of the distribution of the stars with respect to the gas has been considered in a simplified way by a few authors ([31], [2]) who modelled giant H II regions as aggregates of single star Strömgren spheres rather than entities ionized by a dense star cluster located in their center, as is done in most studies. There is an increasing number of objects (e.g. 30 Doradus [16], NGC 1569 [8], I Zw 18 [15]) where the position of individual stars is known, and different situations exist.

So far, the influence of the density distribution has not been much studied. This partly stems from the fact that most photoionization codes assume spherical symmetry [9]. However, even in such a case, there is room for exploration, as seen below.

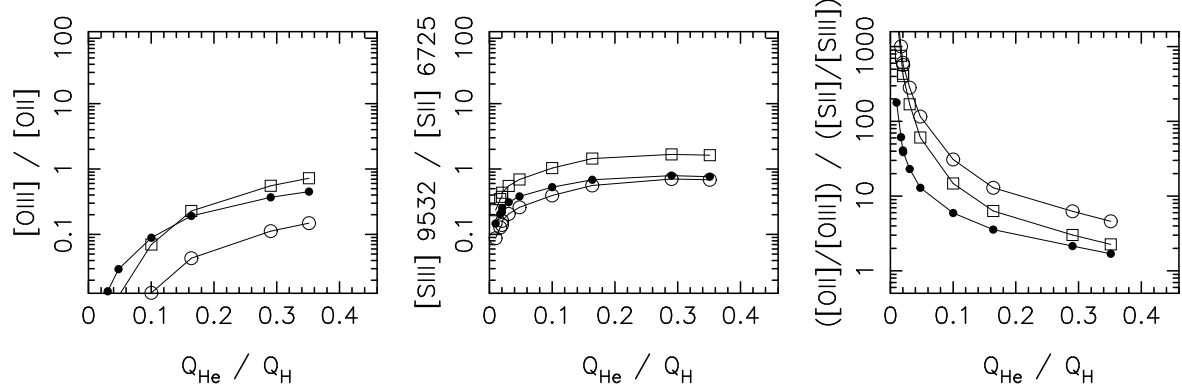


Figure 1: Emission line ratios as a function of Q_{H^o} / Q_{He^o} in sequences of photoionization models for evolving starbursts at $Z = 0.1 Z_\odot$ that are identical in all respects except the geometry. Filled circles: full sphere models of uniform gas density; empty circles: hollow sphere models of same U_S as the full sphere models; empty squares: hollow sphere models of same \bar{U} as the full sphere models.

3 The effect of the density structure on emission line ratios

Here, we will briefly explore several simple geometries, using models obtained with the photoionization code PHOTO and a synthetic evolving starburst as described in Stasińska & Leitherer [35]. A more extended grid of models than the one presented in that paper has now been constructed. The details of all the models, including the intensities of about a hundred of lines from the far IR to the UV and other helpful parameters are available by anonymous ftp from <ftp://obspm.fr/pub/obs/grazyna/cd-crete>.

3.1 Filled sphere versus hollow shell

Two geometries have been mostly used to model giant H II regions. One is a full sphere of constant density (e.g. [35]) or uniformly filled with gas clumps of constant density (e.g. [22]). It has been shown on various occasions that any combination of Q_{H^o} , n , and the filling factor ϵ keeping the ionization parameter U_S constant results in the same nebular ionization structure. A few authors have used another geometry, namely a hollow shell (e.g. [11]). This choice is motivated by the ring structures often seen in giant H II regions in nearby galaxies ([3], [28], [44]) and by the idea that the interaction of stellar winds and supernovae explosions from the central star cluster with the ambient interstellar gas creates large bubbles [4], [21].

In order to illustrate the role played by geometry, we compare in Fig. 1 several line intensity ratios as a function of Q_{He^o}/Q_{H^o} for three sequences of evolving models of giant H II regions identical in every respect except the geometry. Filled circles represent full sphere models. Empty circles represent hollow sphere models of same U_S . Empty squares represent hollow sphere models of same volume averaged ionization parameter \bar{U} as the full sphere models (as mentioned by [22], for a full sphere of constant density and given filling factor, one has $\bar{U} = 3U_S$). It is clearly seen that the emission line spectra are different in all three models. At a given Q_{He^o}/Q_{H^o} , the $[\text{OIII}]/[\text{OII}]$ or $[\text{SIII}]/[\text{SII}]$ ratios are not simply dependent of the "ionization parameter" (whatever definition one takes), and in the example shown in Fig. 1, the dependence on the geometry is not the same for the two line ratios. As a consequence, the "radiation softness parameter" $([\text{OII}]/[\text{OIII}]) / ([\text{SII}]/[\text{SIII}])$ used for ranking the mean effective temperature of H II regions and believed to be relatively insensitive to ionization conditions [42], does depend on the geometry.

Unfortunately, there is no easy rule to predict the magnitude and even the direction of the

changes when altering the geometry, even in such simple cases as considered here. Therefore, unless something is known about the geometry of the H II regions one is studying, it is highly recommended to test the robustness of the inferences derived from photoionization mmodels by considering several exemplary geometries.

It is also important to realize that, in ab initio theoretical models of evolving starbursts, the prescription adopted for the geometry has an incidence on the evolution of the emission line intensity ratios.

García-Vargas et al. [11] adopted a thin shell geometry defined by a distance to the central star cluster held constant during the whole evolution of the cluster. In such a circumstance, we have $\bar{U} \propto Q_{H^{\circ}}(t)$. Stasińska & Leitherer [35] adopted a full sphere geometry of uniform density, and in such a case it is easily shown that $\bar{U} \propto (Q_{H^{\circ}}(t))^{\frac{1}{3}}$. That is, the ionization parameter decreases with $Q_{H^{\circ}}$ (and therefore with time) at a much slower rate than in the models of García-Vargas et al. Clearly, any inference on starburst ages based on such models strongly depends on the adopted nebular properties. So, one cannot simply use the ionization parameter as a measure of the age of a given starburst, as suggested by García-Vargas et al. Actually, a starburst can possibly be unveiled using emission line intensities of the surrounding H II region only if additional information is available.

Note that, if, adopting a thin shell model, the radius were taken to vary with time like in the theory of stellar wind bubbles ([7]), one would have $\bar{U} \propto t^{-\frac{6}{5}} Q_{H^{\circ}}(t)$. On the other hand, adopting a full sphere geometry, if gas were supposed to expand at constant velocity, one would have $\bar{U} \propto t^{-1} (Q_{H^{\circ}}(t))^{\frac{1}{3}}$. Of course, probably none of these two descriptions is realistic, although it is likely that the the ionization parameter decreases with time not only on the account of a decrease in $Q_{H^{\circ}}$ but also because of ram pressure effects and gas dissipation.

3.2 Integrated spectra of core-halo H II regions

There is ample documentation that many giant H II regions exhibit a core-halo structure. There is also evidence, in galaxies, for the existence of a diffuse ionized medium ([32], [43], [24], [25]). This diffuse gas is probably ionized by photons leaking out from the core H II regions, although other mechanisms may be at work in addition [24]. In such a picture, the core is either density bounded, at least in some directions, or ionization bounded with a covering factor less than one. The diffuse medium has a much lower ionization parameter than the core, therefore it emits strongly in [SII] and [OI] and weakly in [OIII]. When studying a nearby giant H II region, the diffuse ionized medium will hardly contribute to the observed spectrum. On the other hand, when observing a galaxy at high redshift, the slit will encompass the bright core together with the diffuse halo, and the resulting spectrum will be very different from that of an H II region in a nearby galaxy [19]. This "aperture effect" can be mistaken for a sign of "activity" or shock excitation in galaxies at large redshifts. An example of such a situation is shown in Table 1 and in Fig. 2.

4 Abundances from the strong line method

While abundances in H II regions are readily obtained from line intensity ratios using electron temperature based empirical methods (the problem of temperature fluctuations should be kept in mind however, see [30], [27], [37] and references therein), these methods cannot be used for distant or low surface brightness galaxies. Indeed, they require a measurement of the faint [OIII] $\lambda 4363$ line. Even in close by H II regions, they cannot be used if the metallicity is higher than about half solar, because the electron temperature is then too low for [OIII] $\lambda 4363$ to be emitted.

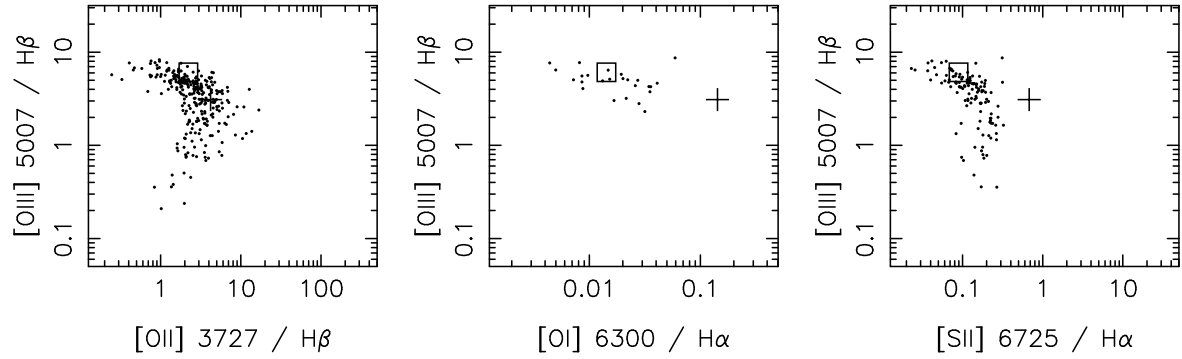


Figure 2: Diagnostic diagrams commonly used to detect signs of activity in giant H II regions and in emission line galaxies. The dots represent the giant H II regions observed in nearby galaxies by Mc Call et al. [20]. The square and the cross show the position the model giant H II regions described in Table 1. The square corresponds to the bright core, the cross corresponds to the integrated spectrum of a "core + halo" structure. In the [OIII]/ H β versus [OI]/ H α and [OIII]/ H β versus [SII]/ H α diagrams, the core + halo is shifted outside the H II region sequence towards the domain of liners.

Table 1: observing a core-halo H II galaxy at different redshifts

starburst parameters: $10^6 M_{\odot}$, $Z = Z_{\odot}/4$, ($Q_{H^2} = 7.7 \cdot 10^{52} \text{ s}^{-1}$)		
	<i>core</i>	<i>halo</i>
n	$100 \text{ (cm}^{-3}\text{)}$	$1 \text{ (cm}^{-3}\text{)}$
ϵ	10^{-2}	10^{-4}
U_S	$2.5 \cdot 10^{-3}$	$2.5 \cdot 10^{-5}$
R_S	300 pc	30 Kpc
M_{ion} (50% covering)	$2 \cdot 10^6 M_{\odot}$	$2 \cdot 10^8 M_{\odot}$
$L(H\beta)$ (50% covering)	$2 \cdot 10^{40} \text{ erg s}^{-1}$	$2 \cdot 10^{40} \text{ erg s}^{-1}$
at 10 Mpc (z=0.002)		
angular radius θ	6"	600"
$F(H\beta)$	$2 \cdot 10^{-12} \text{ (erg cm}^{-2} \text{ s}^{-1}\text{)}$	$2 \cdot 10^{-12} \text{ (erg cm}^{-2} \text{ s}^{-1}\text{)}$
$[OII] \lambda 3727 / H\beta$	2.22	6.24
$[OIII] \lambda 5007 / H\beta$	6.09	0.16
$[OI] \lambda 6300 / H\beta$	0.04	0.77
$[SII] \lambda 6725 / H\beta$	0.25	3.48
at 1000 Mpc (z=0.2)		
angular radius θ	0.06 "	6 "
$F(H\beta)$	$2 \cdot 10^{-16} \text{ (erg cm}^{-2} \text{ s}^{-1}\text{)}$	$2 \cdot 10^{-16} \text{ (erg cm}^{-2} \text{ s}^{-1}\text{)}$
<i>core + halo</i>		
$[OII] \lambda 3727 / H\beta$	4.2	
$[OIII] \lambda 5007 / H\beta$	3.1	
$[OI] \lambda 6300 / H\beta$	0.4	
$[SII] \lambda 6725 / H\beta$	1.9	

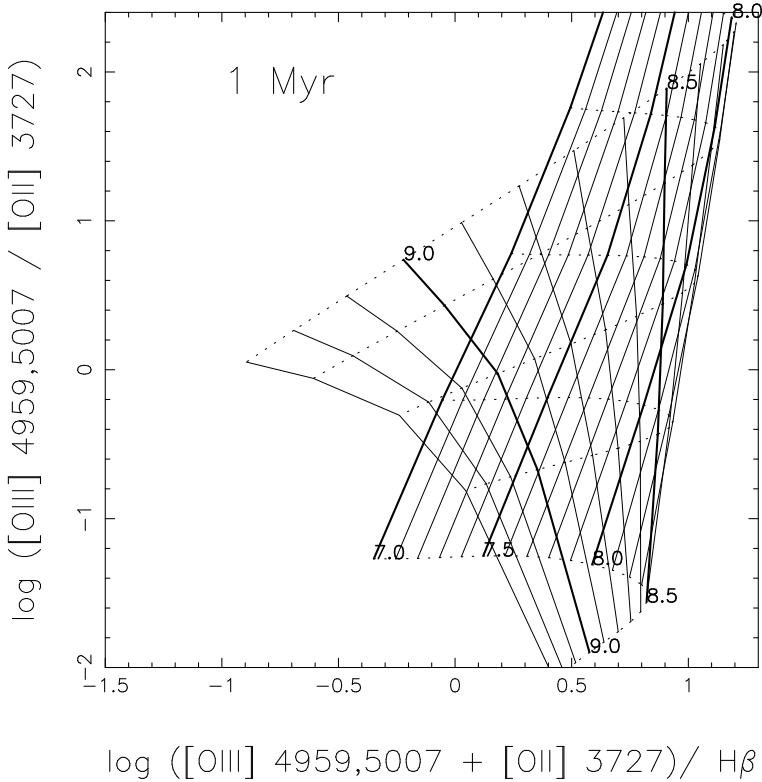


Figure 3: Mc Gaugh's diagram for a giant H II region ionized by a 1 Myr old star cluster as computed using the full sphere photoionization models of [35]. The continuous lines correspond to loci of same O/H by intervals of 0.1 dex in $\log (\text{O/H})$ and are labelled with the value of $\log (\text{O/H})+12$. The dotted lines correspond to loci of same total mass of the starburst, by intervals of 3 dex (corresponding to 1 dex in U_S).

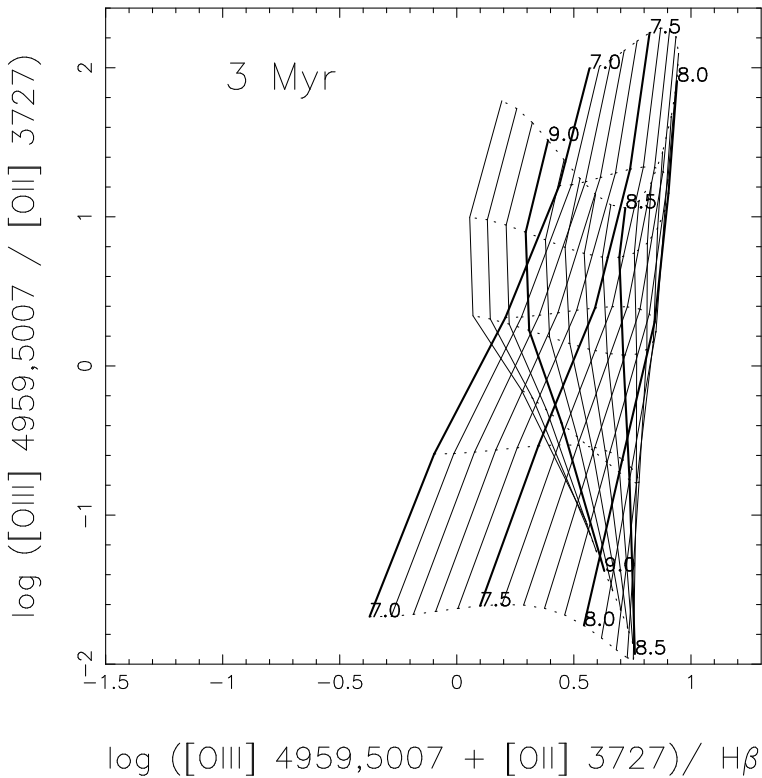


Figure 4: Same as Fig. 3, but for a 3 Myr old star cluster.

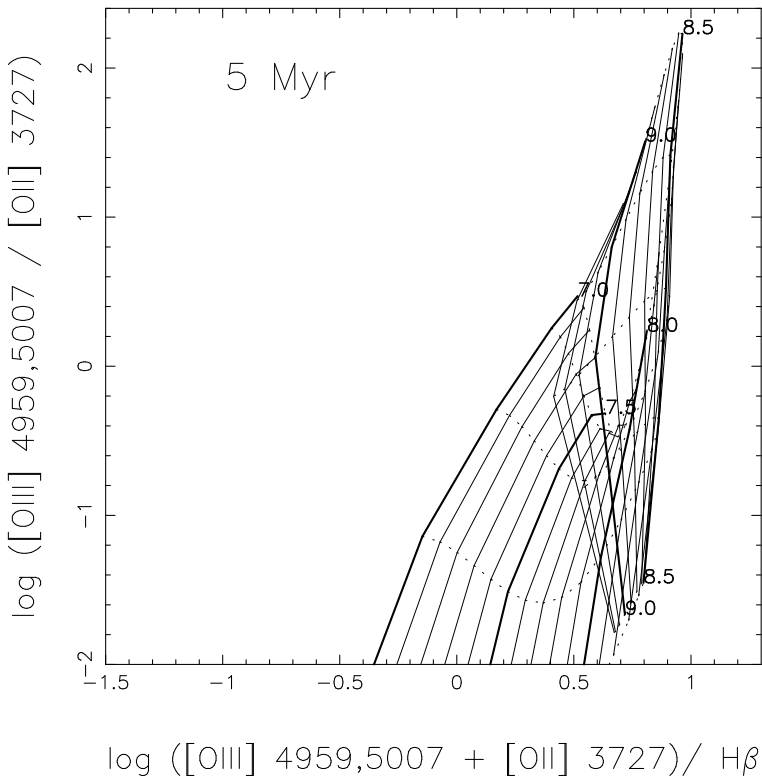


Figure 5: Same as Fig. 3, but for a 5 Myr old star cluster.

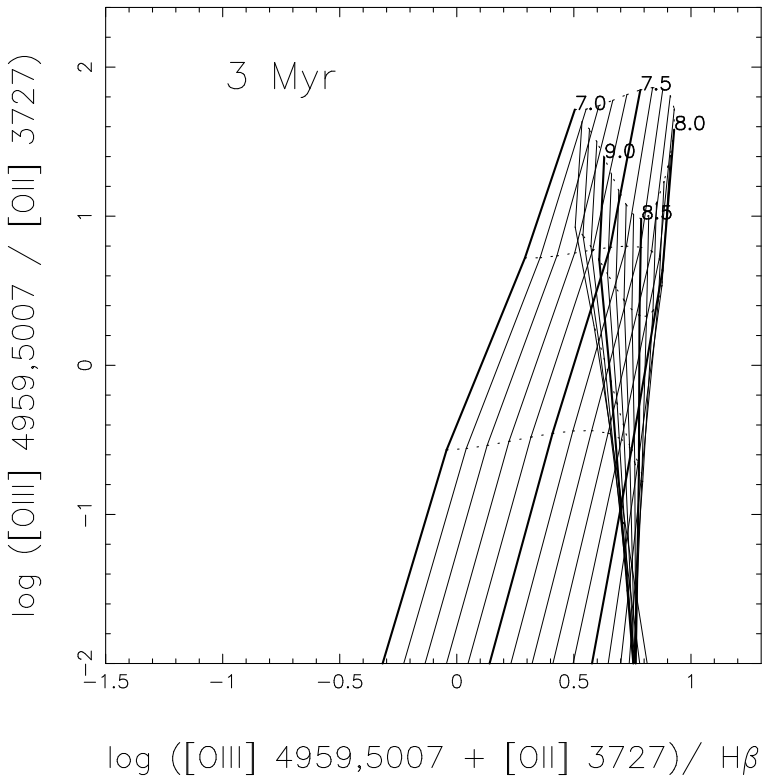


Figure 6: Same as Fig. 4, but for a different nebular geometry: hollow spheres.

An interesting alternative to overcome this problem has been proposed by Pagel et al. [29], using only the strongest lines. Initially, the method was intended to allow the determination of abundances in the metal rich giant H II regions in the inner parts of spiral galaxies. This method has been further discussed in a number of papers (e.g. [20], [6]). Then, Skillman [34] showed its potential use for low abundance systems. Mc Gaugh ([22], [23]) provided the first two-dimensional calibration taking explicitly into account the role of the ionization parameter.

The leading idea is that, with two line ratios ($[\text{OII}]/\text{H}\beta$ and $[\text{OIII}]/\text{H}\beta$) it is possible to estimate the three main defining parameters of an H II region (O/H , $\langle T_{\text{eff}} \rangle$ and \bar{U}) if there is a universal link between these parameters. And indeed, it seems that the initial mass function of the ionizing stars of giant H II regions is universal (see Leitherer, this volume). This implies that, on average, one expects $\langle T_{\text{eff}} \rangle$ and O/H to be related in such objects.

Mc Gaugh has built a grid of photoionization models of various metallicities and ionization parameters ionized by clusters of OB stars, and provided a convenient diagram to read out the values of \bar{U} and O/H from $[\text{OIII}] / [\text{OII}]$ versus $([\text{OIII}] + [\text{OII}]) / \text{H}\beta$. One problem is that the relation between $([\text{OIII}] + [\text{OII}]) / \text{H}\beta$ and O/H is double valued: at low metallicities, the intensities of $[\text{OII}]$ and $[\text{OIII}]$ with respect to $\text{H}\beta$ increase with increasing O/H . But when the oxygen abundance gets high enough for this element to become the main coolant, the electron temperature drops and the cooling is gradually transferred from the optical forbidden lines to the infra red fine structure lines. Consequently, $([\text{OIII}] + [\text{OII}]) / \text{H}\beta$ becomes a decreasing function of O/H . If nothing is suspected a priori about the metallicity of an object, one can use $[\text{NII}] / [\text{OII}]$ as a discriminant between the two regimes: this ratio is expected to be small (< 0.1) at low metallicities [23].

Mc Gaugh analyzed various sources of errors in the method and estimated an intrinsic uncertainty of 0.05 dex in $\log(\text{O/H})$ at the low abundance end, 0.1 dex at the high abundance end, and 0.2 dex in the turn over region. The expected overall uncertainties in the oxygen abundance are obtained by combining these formal error bars with those due to observational errors [23], giving an estimated accuracy of about 0.2 dex for reasonably high signal-to-noise data, and worse in the turn over region.

Note that, on the low abundance end, comparing the values of O/H derived from the strong line method and from the electron temperature based method provides a direct estimate of the error. Unfortunately, this cannot be done on the high abundance end. Even tailored photoionization models of metal rich H II regions fitting all the important lines do not provide a reliable calibration: the observational constraints are generally far from sufficient to allow a precise determination of the oxygen abundance in metal rich objects where, as developed below, the emission line intensities are extremely sensitive to the physical conditions in the nebulae.

Mc Gaugh's computations were done assuming a zero age starburst of given upper stellar mass limit, M_{up} . The evolution of a starburst was mimicked by considering different values of M_{up} . Mc Gaugh's diagram is constructed for $M_{\text{up}} = 60 M_{\odot}$, corresponding to an average age of ~ 3 Myr for a burst having initially $M_{\text{up}} = 100 M_{\odot}$.

Using evolving synthetic starburst models [18], it is possible to follow the distortion of Mc Gaugh's diagram as the starburst ages. This is done in Figs. 3, 4 and 5, which show the diagram obtained by bicubic spline interpolation on the grid of photoionization models of [35] at 1 Myr, 3 Myr and 5 Myr respectively. The continuous lines correspond to loci of same O/H , while the dotted lines correspond to loci of same total initial mass of the stars (and not same ionization parameter as in Mc Gaugh).

We see that, on the low abundance end, the main effect of ageing is a drop in $[\text{OIII}] / [\text{OII}]$, which is due to a decrease of \bar{U} implied by the lowering of the number of ionizing photons. The isoabundance curves are not much displaced, especially at low excitation. Indeed, in this regime, cooling is mainly due to collisional excitation of H Ly α and is a steep function of

the electron temperature. Therefore, the electron temperature is insensitive to changes in the heating rate, and so are the intensities of the [OIII] $\lambda 5007$ and [OII] $\lambda 3727$. As a consequence, the oxygen abundance derived from such a diagram is not too dependent on age. A typical value of the corresponding uncertainty is ± 0.1 dex for an age of 3 ± 1 Myr.

On the high abundance end, the distortion of Mc Gaugh's diagram is impressive. At high metallicities, cooling is provided by the infrared fine structure lines [OIII] $\lambda\lambda 52, 88\mu$, which are insensitive to the electron temperature. Therefore, the electron temperature is extremely affected by changes in the energy gains, and so is the intensity of [OIII] $\lambda 5007$. To make things worse, at high metallicities, the mean effective temperature of the stellar radiation is subject to large variations during the evolution (see Table 3 of [35]). An important hardening occurs when stars reach the Wolf-Rayet phase, boosting the [OIII] $\lambda 5007$ line. As a result, oxygen abundances derived from the strong line method are quite uncertain at the high metallicity end. Typically, an H II region having $\log(O/H)+12 = 9$ and an age of 5 Myr would appear less metal rich by 0.3 dex if interpreted with a diagram corresponding to 3 Myr. Other sources of uncertainties contribute as well, owing to the fact that the electron temperature is so ill defined. For example, any density irregularity, any change in the geometry will greatly affect the emission in [OIII] $\lambda 5007$. An example is shown in Fig. 6, which presents Mc Gaugh's diagram at 3 Myr like Fig. 4, but for hollow spheres of same \bar{U} as the full sphere models used in Fig. 4. Note that Figs. 3 – 6 were constructed by extrapolating the solar metallicity models towards higher abundances. We have also constructed models at twice solar metallicity (they are available on the ftp site mentioned above). Using these models produces very twisted isoabundance curves even around $\log(O/H)+12 = 9$, because at metallicities twice solar, the strong cooling may completely quench the [OIII] $\lambda 5007$ line. The diagram is further complicated by the fact that, at high metallicities, recombination takes over collisional excitation in the production of the [OII] line.

As regards the turnover region, warnings have already been expressed by several authors. In this regime, the main cooling agent is [OIII] $\lambda 5007$, therefore the intensity of this line is independent of O/H, and is a function of the heating rate only. Nevertheless, one can say that an H II regions showing $([OIII]+[OII])/H\beta > 0.7$ must have a $\log(O/H)+12$ within a few dex of 8.

In summary, the strong line method is rather robust at low abundances ($\log(O/H)+12 < 7.7$) but is rather uncertain at higher metallicities. The fact that in spiral galaxies, one does see a trend in $([OIII]+[OII])/H\beta$ with galactocentric radius (e.g. [17]) is probably indeed related to an abundance effect. In this case, observing a large number of H II regions at a given galactocentric radius will smooth out the effects due to non uniformity of the stellar populations. Still, the unknown geometry of the H II regions affects any calibration of the method. Trustworthy abundance determinations in metal rich H II regions have to await the observation of the infrared fine structure lines.

It has been suggested [39] that the line ratio [AIII] $\lambda 7136$ / [SIII] $\lambda 9532$ could be an indicator of metallicity in metal rich object, being an indicator of electron temperature. We do not share this optimistic view since, as commented above, the electron temperature is ill defined at high metallicities and strongly dependent on the properties of the ionizing clusters and on the density structure of the nebulae.

The determination of the N/O ratio has been specifically discussed by several authors [41], [40], with the help of single star photoionization models. Using the grid of models for evolving starburst presented in Sect. 3 as an interpolating device, one can obtain the N/O ratios from the observed [NII] / [OII] with a typical uncertainty of ± 0.15 dex.

References

- [1] Baldwin J.A., Ferland G.J., Martin P.G. et al, 1991, *Astrophys. J.* **374**, 580
- [2] Barbaro C., Poggianti B.M., 1997, *Astr. Astrophys.* **324**, 490
- [3] Chu Y.H., Mc Low M-M., *Astrophys. J.* **365**, 510
- [4] Castor J., McCray R., Weaver R., 1975, *Astrophys. J.* **200**, L107
- [5] Cerviño M., Mas-Hesse J.M., 1994, *Astr. Astrophys.* **284**, 749
- [6] Dopita M.A., Evans I.N., 1986, *Astrophys. J.* **307**, 431
- [7] Dyson J.E., 1979, *Astr. Astrophys.* **73**, 132
- [8] De Marchi G., Clampin M., Greggio L. et al., 1997, *Astrophys. J.* **479**, L27
- [9] Ferland G.J. et al., 1995, in *Analysis of Emission Lines: a Meeting Honoring the 70th Birthdays of D.E. Osterbrock and M.J. Seaton*, eds. R.E. Williams & M. Livio (Cambridge Univ. Press), 83
- [10] García-Vargas, M. L., Díaz, 1994, *Astrophys. J. Suppl. Ser.* **91**, 553
- [11] García-Vargas, M. L., Bressan, A., Díaz, A.I., 1995, *Astr. Astrophys. Suppl. Ser.* **112**, 13
- [12] García-Vargas, M. L., 1996, in *From Stars to Galaxies*, ASP Conf. Series, Vol. 98, eds. C. Leitherer, U. Fritze-v. Alvensleben, and J. Huchra, 244
- [13] Garnett D.R., Skillman E.D., Dufour R.J. et al., *Astrophys. J.* **443**, 64 76
- [14] Henry, R.B.C., 1993, *MNRAS* **261**, 306
- [15] Hunter D.A., Thronson H.A. Jr., 1995, *Astrophys. J.* **452**, 238
- [16] Hunter D.A., Shaya E.J., Scowen P., et al, 1995, *Astrophys. J.* **444**, 758
- [17] Kennicutt R.C., Garnett D.R., 1996, *Astrophys. J.* **456**, 504
- [18] Leitherer C., Heckman T.M., 1995, *Astrophys. J. Suppl. Ser.* **96**, 9
- [19] Lehnert M.D., Heckman T.M., 1994, *Astrophys. J.* **426**, L27
- [20] Mc Call M.L., Rybski P.M., Shields G.A., 1985, *Astrophys. J. Suppl. Ser.* **57**, 1
- [21] Mc Cray R., Kafatos M.C., 1987, *Astrophys. J.* **317**, 190
- [22] Mc Gaugh S.S., 1991, *Astrophys. J.* **380**, 140
- [23] Mc Gaugh S.S., 1994, *Astrophys. J.* **426**, 135
- [24] Martin C.L., 1997, *Astrophys. J.* **491**, 561
- [25] Martin C.L., Kennicutt R.L., 1997, *Astrophys. J.* **483**, 698
- [26] Mathis J.S., 1986, *PASP* **98**, 995
- [27] Mathis J.S., 1995, *Rev Mex AA (Serie de Conferencias)* **3**, 207
- [28] Oey M.S., Massey P., 1994, *Astrophys. J.* **425**, 635
- [29] Pagel B.E.J., Edmunds M.G., Blackwell D.E. et al., 1979, *MNRAS* **189**, 95
- [30] Peimbert M., 1995, in *The Analysis of Emission Lines*, eds. Williams. R.E., Livio M. , Cambridge University Press p. 165
- [31] Peña M., 1986, *PASP* **98**, 1061
- [32] Rand R.J., 1996, *Astrophys. J.* **462**, 712
- [33] Shields J.C., Kennicutt R.C., 1995, *Astrophys. J.* **454**, 807
- [34] Skillman E.D., 1989, *Astrophys. J.* **347**, 883
- [35] Stasińska G., Leitherer C., 1996, *Astrophys. J. Suppl. Ser.* **107**, 661
- [36] Stasińska G., 1996, in *From Stars to Galaxies*, ASP Conf. Series, Vol. 98, eds. C. Leitherer, U. Fritze-v. Alvensleben, and J. Huchra, 232
- [37] Stasińska G., 1998, in *Abundance profiles: diagnostic tools for galaxy history*, ASP Conf. Ser., eds. Friedli et al. in press
- [38] Stasińska G., Schaefer D., 1997, *Astr. Astrophys.* **322**, 615
- [39] Stevenson C.C., Mac Call M.L., Welch D.L., 1993, *Astrophys. J.* **408**, 460

- [40] Thurston T.R., Edmunds M.G., Henry R.B.C., 1996, *MNRAS* **283**, 990
- [41] Vila-Costas M.B., Edmunds M.G., 1993, *MNRAS* **265**, 199
- [42] Vilchez J.M., Pagel B.E.J., 1988, *MNRAS* **231**, 257
- [43] Wang J., Heckman T.M., Lehnert M.D., 1997, *Astrophys. J.* **491**, 114
- [44] Yang H., Chu Y.H., Skillman E.D., Terlevich R., 1996, *Astronom. J.* **112**, 146